MOLECULAR PHYSICS, 1991, VOL. 72, NO. 4, 831–846

Non-equilibrium molecular dynamics simulations of structured molecules

Part I. Isomeric effects on the viscosity of butanes

By RICHARD L. ROWLEY† and JAMES F. ELY
National Institute of Standards and Technology, Boulder, Colorado, 80303, U.S.A.

(*Received 13 August 1990; accepted 10 October 1990*)

Corresponding-states theories fail to predict the large difference observed between n-butane and isobutane viscosities at similar reduced conditions. To investigate the molecular cause of these structural effects upon viscosity, non-equilibrium molecular dynamics simulations of Lennard-Jones site–site models representing n-butane and isobutane are performed over much of the density range for which experimental data are available. Simulated viscosities at zero shear agree very well with experimental data over the entire density range. Site size, non-equilibrium molecular alignment and molecular geometry are the primary factors causing both the similarities and differences between the isomers' viscosity and rheology.

1. Introduction

Extended corresponding states (CS) techniques such as TRAPP [1] and ELK [2] have proved to be very effective in the calculation of thermophysical properties of a wide range of fluids. In view of this general applicability, it is perhaps somewhat surprising that substantial errors result when these methods are used to calculate high-density liquid viscosities of some of the simplest branched alkanes. Most physical and thermodynamic properties are not radically affected by chain branching, but the liquid viscosity of branched small-carbon-number alkanes is substantially different from that of the corresponding normal alkane, particularly at high densities. This difference in viscosity between isomers is not accurately reflected in current CS methods, as is evident in figure 1. While TRAPP predictions are seen to be quite accurate for n-butane over the entire density range, errors up to 200% in predicted viscosities of isobutane are observed at the highest densities. At least in this case, molecular structure appears to affect the viscosity differently than the other thermophysical properties commonly calculated from CS methods. It therefore seems appropriate to perform molecular dynamics (MD) simulations to study the molecular origins of these isomeric effects upon liquid viscosity in an effort to provide insights useful for eventual improvement of CS methodologies.

n-Butane and isobutane were chosen as the simplest representative example of the problem illustrated above. Non-equilibrium molecular dynamics (NEMD) simulations of their viscosity over a wide range of liquid densities were performed for direct

† Permanent address: Department of Chemical Engineering, 350CB, Brigham Young University, Provo, Utah 84602, U.S.A.

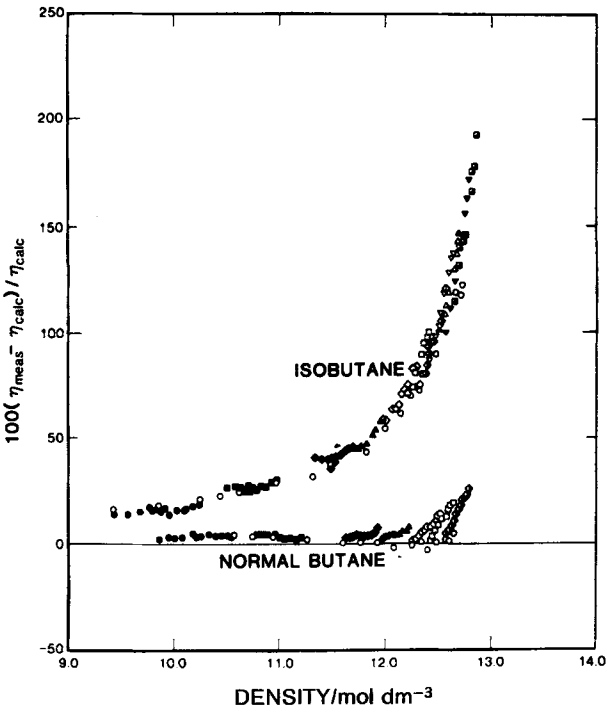

Figure 1. Failure of CS method to predict the variation in viscosity due to structural differences between n-butane and isobutane. Different symbols represent different isotherms from 120 K to 300 K. (Reproduced from [3].)

comparison with the experimental data of Diller and Van Poolen [3]. Simulated viscosities agreed remarkably well with experimental values, and analysis of the non-equilibrium structure shows a distinct difference between the rheology of the isomers, which can be used to explain the experimentally observed difference in viscosity between the two fluids.

2. Simulations

2.1. *Molecular models*

An effective four-site model for n-butane molecules has been tested previously and used in MD simulations [4–6]. The model molecule is composed of four equivalent methyl/methylene sites located at carbon centres. Interactions between sites of different molecules were modelled with standard 12–6 Lennard-Jones (LJ) potentials. Distances between neighbouring sites were constrained to 0·153 nm, and bond angles were fixed at 109·47° by a next-nearest-neighbour distance constraint. All intramolecular interactions were obtained from the Ryckaert–Bellemans [4] potential, which has proved to be effective in modelling conformational populations and interconversions [4–8]. Table 1 summarizes the model parameters used. While slightly different values of the LJ parameters have also been used in simulations of n-butane [7–11], the values in table 1 were selected because of the excellent representation of viscosity obtained by Edberg *et al.* [5, 6].

Isobutane was similarly modelled with four equivalent LJ sites located at the

Table 1. Model parameters.

Parameter	n-Butane	Isobutane	
		Model I	Model II
m/kg	$2{\cdot}41 \times 10^{-26}$	$2{\cdot}41 \times 10^{-26}$	$2{\cdot}41 \times 10^{-26}$
d (bond distance)/nm	0·153	0·153	0·153
Θ (bond angle)	109·47°	109·47°	109·47°
ε/k (LJ energy parameter)/K	72	72	72
σ (LJ distance parameter)/nm	0·3923	0·3923	0·4020

physical carbon centres. However, in terms of parameter values, two different models were used for isobutane, as shown in table 1. Model I is identical with that used for n-butane, and it is therefore useful for comparison of simulations performed at the same corresponding conditions for the two fluids. Simulations based on model II, on the other hand, represent the experimental viscosity data better. In fact, the model II value of σ was selected on the basis of agreement between simulated values obtained using various σ values and the experimental datum at a single density. A larger σ value for isobutane is consistent with previous findings in which an optimized σ value for CH_3 in isobutane was found to be slightly larger than that found for the CH_3 and CH_2 groups in n-butane [12]. Since most of the intermolecular potential energy is due to interactions between outer CH_3 groups, the generic CH_3/CH_2 σ is expected to be larger for isobutane. As in the case of n-butane, isobutane molecules were considered rigid with bond lengths and angles fixed at the values shown in table 1.

2.2. *MD simulations*

Non-equilibrium MD simulations were performed using a *NVT* (canonical ensemble) algorithm developed by Edberg *et al.* [5], a molecular version of the isothermal shear algorithm known as SLLOD [13, 14]. Rather than solve Newtonian equations of motion subject to constraints as popularized by the SHAKE algorithm [15], non-Newtonian equations of motion that include the constraint forces naturally are derived following the prescription of Gauss's principle of least constraints [5, 14, 16]. A principal advantage of this method for the type of problem considered here is that all of the constraints imposed by the fixed bond distances, the isothermal thermostat and the applied shear field are similarly and efficiently incorporated into the equations of motion as additional force terms. This makes implementation of the method into standard MD programs relatively straightforward. Newtonian forces $\boldsymbol{F}^{\mathrm{N}}$, can be calculated from relative site positions in the standard way, the constraint forces $\boldsymbol{F}^{\mathrm{C}}$ can be obtained from Gauss's principle, and the usual integration algorithms may be used to trace the particle trajectories in phase space using the total force $\boldsymbol{F}^{\mathrm{N}} + \boldsymbol{F}^{\mathrm{C}}$. Derivation of the appropriately constrained equations of motion and their implementation into standard MD codes are adequately discussed in [5, 6].

NVT simulations were performed on three-dimensional systems of 125 molecules using a cut-off distance of $2{\cdot}5\sigma$ with appropriate long-range corrections. The geometry used is schematically shown in figure 2, and the constant applied shear rate γ in the simulations is defined with respect to these Cartesian coordinates and the x component of velocity as

$$\gamma = \frac{\partial v_x}{\partial y}. \tag{1}$$

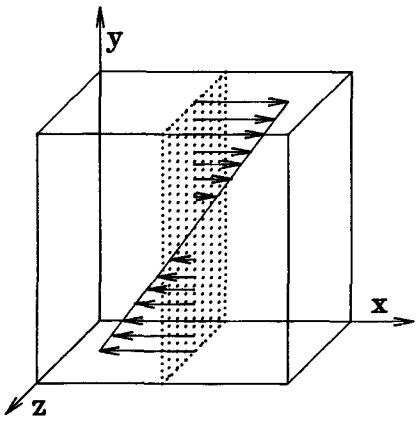

Figure 2. Schematic showing the linear velocity profile or constant shear rate in relation to the coordinate system used in the simulations.

All simulations were performed on a Cyber 205† supercomputer using the automatic vectorization options of the resident Fortran compiler. The dimensionless time step size was chosen to be 0·0015, corresponding to 2·9 fs in real time. Between 60 000 and 120 000 time steps beyond 'equilibration' were used to obtain property time averages. All production runs were started from configuration files of previous simulations by changing the run conditions or shear rate. This generally shortened the time required to 'equilibrate' or stabilize the simulated properties to about 20 000 time steps.

NEMD simulation of the viscosity of two structured fluids over a range of densities is an ambitious task. Previous NEMD studies of structured molecules have generally been restricted to a few conditions for a single fluid. This is because computer time requirements are roughly proportional to Q^2, where Q is the number of sites used to represent the molecule. Moreover, simulations must be performed at several shear rates in order to accurately extrapolate to zero applied shear. Reduced time steps and long simulations are often required to maintain stability and to compute accurate properties as a direct result of the increased number of degrees of freedom. Therefore it was expedient to significantly modify a previous code [5] by implementation of time-saving features in order to make this study tractable. While none of these time-saving methods are new, their application to constraint NEMD algorithms, particularly in combination with each other, is unique. The final code ran about 11 times faster than the original. The algorithms and their time-saving benefits are described below.

(i) The Runge–Kutta integration method used in the original code was replaced by a fourth-order predictor–corrector (PC) method to avoid multiple force calculations per time step. It was also found that the predictor–corrector method made the integration more stable, permitting a 50% increase in the small step size generally required by the constraint algorithm. There is a trade-off between larger step size and the increasing frequency at which bond lengths must be re-optimized through

† Brand names and commercial sources of materials and instruments are given for scientific completeness and comparison purposes. Such information does not constitute endorsement of these products or imply their superiority over other available brands.

the penalty functions. The stability of the PC algorithm permitted the increased step size without increasing the frequency at which the penalty functions were exceeded.

(ii) A neighbour list (NL) with automatic update was also implemented. Because of the boundary conditions used in the SLLOD algorithm, neighbour lists have proved difficult to implement. In this work the SLLOD periodic boundaries were applied to the centres of mass of the molecules. When a molecule crosses a cell boundary in the y direction, the x coordinate of the image particle inserted through the opposite y boundary is shifted by an amount that depends upon the relative time and shear that has occurred. If a regular neighbour update time is used, a particle may be shifted into a new neighbourhood list between updates by this SLLOD boundary condition. It is therefore essential that the update be performed automatically as necessary, rather than at preset intervals. In this work a spherical neighbourhood buffer radius was taken as $r_c + 0{\cdot}3\sigma$, where r_c is the potential cut-off distance ($2{\cdot}5\sigma$ here). For each molecule, centre of mass displacements were vectorally added at each time step and the maximum displacement since the last neighbour update was determined. The displacement vectors also included effects due to shear and shift imposed by y-boundary crossings. This is essential since the SLLOD periodic boundary condition may shift the x coordinate of a molecule by any fraction of the cell length when it crosses the y boundary. When twice the maximum displacement exceeded the neighbour buffer distance, a neighbour update was initiated. The effectiveness of the neighbour list depends considerably upon the shear rate and temperature of the simulation. Larger temperatures and higher shear rates require updates more frequently. At the lower shear rates the neighbour list required updating only about every 30 time steps, while average updates were required two to three times more frequently at the higher shear rates.

(iii) A multiple time step (MTS) method [17] was also introduced to minimize the time spent evaluating pair forces in the main force loop. The Newtonian force on a molecule can be divided into primary, $\boldsymbol{F}^{\mathrm{p}}$, and secondary, $\boldsymbol{F}^{\mathrm{s}}$, forces. Neighbours of a molecule are considered primary if they are within a distance r_{p}. In this work r_{p} was taken as $1{\cdot}2\sigma$. The dynamics of a molecule is dominated by its primary neighbours. It feels a rapidly changing primary force resulting from collisions with its nearest neighbour or 'cage' molecules and a weaker secondary force (from molecules for which $r_{\mathrm{p}} < r < r_{\mathrm{c}}$), which changes much more slowly in time. Implementation of the MTS method is straightforward, but does require considerable additional programming. At time t neighbours of each particle are classified as primary or secondary, and all forces are calculated in the normal way. Additionally, the time derivatives of the secondary forces are calculated. This involves little additional computation time, since the derivatives of position required in these calculations are already available from the predictor algorithm. At each of the next m-1 time steps the total secondary Newtonian force on molecule i is estimated from a Taylor series

$$\boldsymbol{F}_i^{\mathrm{s}}[t + m(\delta t)] \approx \boldsymbol{F}_i^{\mathrm{s}}(t) + m\,\delta t\,\dot{\boldsymbol{F}}_i^{\mathrm{s}}(t) + \tfrac{1}{2}m^2(\delta t)^2\ddot{\boldsymbol{F}}_i^{\mathrm{s}}(t). \tag{2}$$

The method in effect uses two separate time steps—the usual δt for updating primary forces and $m\,\delta t$ for explicitly updating secondary forces.

Secondary forces between molecules i and j and their time derivatives are required for implementation of this method. These are calculated from (omitting the subscripts

i and j),

$$\boldsymbol{F}^{s} = A\boldsymbol{r}, \tag{3}$$

$$\dot{\boldsymbol{F}}^{s} = A\dot{\boldsymbol{r}} + B(\boldsymbol{r}\cdot\dot{\boldsymbol{r}})\boldsymbol{r}, \tag{4}$$

$$\ddot{\boldsymbol{F}}^{s} = A\ddot{\boldsymbol{r}} + 2B(\boldsymbol{r}\cdot\dot{\boldsymbol{r}})\dot{\boldsymbol{r}} + \boldsymbol{r}[C(\boldsymbol{r}\cdot\dot{\boldsymbol{r}})^2 + B(\dot{\boldsymbol{r}}\cdot\dot{\boldsymbol{r}} + \boldsymbol{r}\cdot\ddot{\boldsymbol{r}})], \tag{5}$$

where

$$A = -\frac{1}{r}\frac{\mathrm{d}\phi}{\mathrm{d}r}, \qquad B = \frac{1}{r}\frac{\mathrm{d}A}{\mathrm{d}r}, \qquad C = \frac{1}{r}\frac{\mathrm{d}B}{\mathrm{d}r}, \tag{6}$$

and ϕ is the intermolecular pair potential. Also required for implementation of the method are the derivatives of the virial $V = \boldsymbol{F}\cdot\boldsymbol{r}$, because the secondary portion of the virial must also be evaluated from a Taylor series during the shorter steps. These derivatives are

$$\dot{V}_{uv} = \dot{F}_u r_v + F_u \dot{r}_v, \tag{7}$$

$$\ddot{V}_{uv} = \ddot{F}_u r_v + 2\dot{F}_u \dot{r}_v + F_u \ddot{r}_v, \tag{8}$$

where u and v subscripts represent the Cartesian components of the vectors and tensors, and the force and its derivatives are obtained from (3)–(6).

Each modification was individually tested by comparisons with and without the new algorithm for over 50 000 time steps. In this work secondary forces were explicitly re-evaluated every seven steps ($m = 7$). A summary of the relative CPU savings on the supercomputer for each of the above modifications is contained in table 2.

2.3. *Property evaluation*

Bulk properties of the fluid were computed with the standard time averages of appropriate dynamical variables. The temperature of the system is constrained to be a constant of motion given by

$$T = \sum_i \frac{\boldsymbol{p}_i^2}{M(3N-4)k}, \tag{9}$$

where the usual $3N$ degrees of freedom have been reduced by four owing to the requirement of momentum conservation in each of the three directions and the constraint imposed on the sum of squared momenta by the constant-temperature algorithm. The molecular pressure tensor is defined by the virial theorem as

$$\boldsymbol{P} = \frac{1}{V}\sum_i \left(\frac{\boldsymbol{p}_i\boldsymbol{p}_i}{M} + \boldsymbol{r}_i\boldsymbol{F}_i\right). \tag{10}$$

The hydrostatic pressure is obtained from $\frac{1}{3}\mathrm{Tr}(\boldsymbol{P})$, and the nonlinear shear-dependent

Table 2. Relative CPU times for various time-saving algorithms.

Algorithm	CPU time relative to original code
Original code	1·00
PC	0·53
PC + NL	0·35
PC + NL + MTS	0·14
PC + NL + MTS + expanded step size	0·09

Table 3. Approximate numerical relationships between dimensionless and experimental variables.

Property	Relationship
Temperature	$T^* = T/72\,\mathrm{K}$
Molar density	$\rho^* = \rho_m/7\,\mathrm{mol\,dm^{-3}}$
Shear rate	$\gamma^* = \gamma/5 \times 10^{11}\,\mathrm{s^{-1}}$
Viscosity	$\eta^* = \eta/0{\cdot}03\,\mathrm{mPa\,s}$
Time	$t^* = t/1{\cdot}93\,\mathrm{ps}$

viscosity is computed from the constitutive relation

$$\eta(\gamma) = -\frac{1}{\gamma}\langle \tfrac{1}{2}P_{yx} + \tfrac{1}{2}P_{xy}\rangle, \tag{11}$$

where the angle brackets denote a time average. It can be shown from linear response theory that $\eta(\gamma)$ defined in (11) reduces to the standard Green–Kubo relation for the zero-shear-rate viscosity in the limit $\gamma \to 0$ [6]. Thus, extrapolation of $\eta(\gamma)$ to $\gamma = 0$ gives the Green–Kubo viscosity $\eta(0)$. The asymptotic behaviour for $\eta(\gamma)$ [18–20],

$$\eta(\gamma) = \eta(0) - A\gamma^{1/2}, \tag{12}$$

is generally used to perform the extrapolation [20, 21].

Simulations were performed at conditions corresponding to those of available experimental data [3]. Properties were made dimensionless in terms of site parameters. Thus

$$T^* = \frac{kT}{\varepsilon}, \qquad \eta^* = \frac{\eta\sigma^2}{(m\varepsilon)^{1/2}}, \qquad \gamma^* = \gamma\sigma\left(\frac{m}{\varepsilon}\right)^{1/2}. \tag{13}$$

Likewise, the site number density ρ is four times the molecular number density, or

$$\rho^* = \rho\sigma^3 = \frac{4N\sigma^3}{V}. \tag{14}$$

Approximate numerical relationships between dimensionless and experimental variables applicable to this work are given for convenience in table 3.

3. Results

3.1. *Model I for isobutane*

Model I for isobutane was used to make a comparison study of the viscosity of the two fluids at similar reduced conditions. It was also used to provide information about the difference in rheology between the two fluids and to determine an appropriate range of γ^* values over which (12) could be used to obtain $\eta(0)$. Simulations for these purposes were made at $T^* = 1{\cdot}871$ and $\rho^* = 1{\cdot}85$ for both fluids.

To ascertain the dependence of simulated viscosity on shear rate, simulations were performed at several shear rates in the range $0 \leqslant \gamma^* \leqslant 1{\cdot}0$; the results are shown in figure 3. Note that η^* appears quite linear with $\gamma^{*1/2}$ over the range $0 \leqslant \gamma^* \leqslant 0{\cdot}16$, but that the rheology of the two fluids is different for larger values of γ^*. While both fluids are shear-thinning in the low-shear region, η^* seems nearly independent of γ^* in the range $0{\cdot}25 \leqslant \gamma^* \leqslant 1{\cdot}0$. This agrees with previous findings [6] in which a

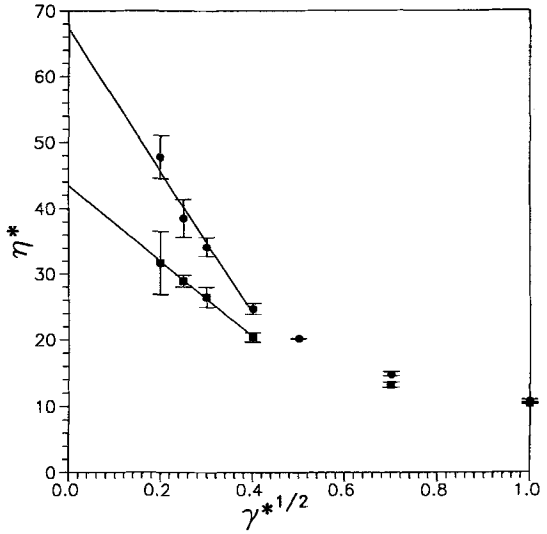

Figure 3. Difference in rheological behaviour of n-butane (●) and isobutane (■) at $T^* = 1{\cdot}871$ and $\rho^* = 1{\cdot}85$. Uncertainty bars are estimated from the standard deviation of shorter sequential simulations.

shear-thinning (for $0 < \gamma^* < 0{\cdot}25$), an approximately Newtonian (for $0{\cdot}25 < \gamma^* < 1$), and a subsequent shear-thinning (for $\gamma^* > 1$) regime were all noted for $\eta(\gamma)$ of n-butane. The rheology of isobutane is seen to be similar to that of n-butane in figure 3, although n-butane is significantly more shear-thinning than isobutane in the first regime. The error bars shown in this figure are only relative estimates calculated from the standard deviations of between four and eight successive 15 000 time-step portions of the total simulation.

The linear fit of (12) shown in figure 3 was obtained from a weighted least squares regression analysis. Interestingly, η^* is smaller for isobutane than n-butane at equivalent reduced conditions. The values at $\gamma^* = 0$ obtained from the simulations are compared with reduced experimental data (made dimensionless with (13) and (14) and the LJ parameter of table 1) in figure 4. It is obvious from this comparison that a purely structural difference in the models cannot account for the observed differences in viscosities of the two fluids. Although branching does affect the viscosity, it lowers it at equivalent reduced conditions relative to its straight-chain counterpart, in apparent contradiction to the observed behaviour. Other factors must outweigh the decrease in reduced viscosity due to branching.

3.2. *Model II for isobutane*

The simulated viscosity of isobutane was found to be quite insensitive to the value of ε/k relative to its dependence on σ. Therefore the isobutane simulations were repeated with different σ values at the test ρ^* (and T^*) shown in figure 3. This is primarily a scaling phenomenon due to the σ^3 and σ^2 dependence, which relates ρ^*, η^* to ρ, η in (13) and (14). Values of η^* obtained from the simulations at a particular ρ^* are fairly insensitive to the chosen value of σ, but the actual ρ and η that correspond to these values are therefore extremely sensitive to σ. This scaling of isobutane with a slightly larger site size parameter reverses the relative locations of the

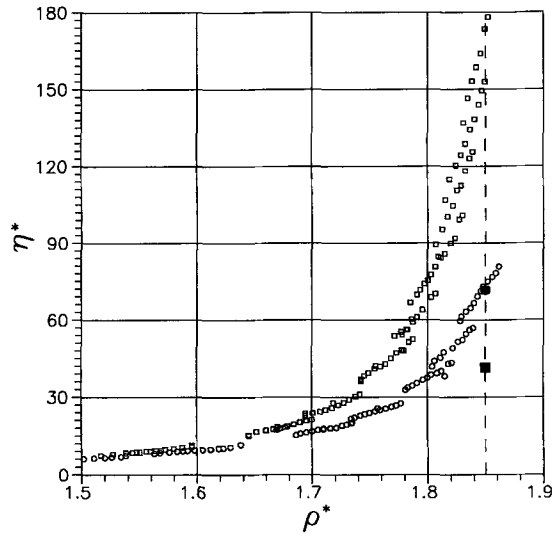

Figure 4. Comparison of simulated (filled symbols) and experimental (empty symbols) reduced viscosities for n-butane (●, ○) and isobutane (■, □). The dashed line shows the comparison at the same reduced conditions as figure 3.

curves shown in figure 3 for the two fluids, bringing into agreement with the simulation the trend of a lower η^* value for the branched molecule at equivalent reduced (in terms of the site LJ parameters) conditions. This procedure was used to select the value of σ shown in table 1 for isobutane model II. The value of σ for model II represents a change of only 2·5% from model I, but the change produces substantially better agreement with experiment.

Values for $\eta^*(0)$ were obtained in this work from a weighted linear least squares fit of simulated values at $\gamma^{*1/2} = 0{\cdot}2$, 0·25, 0·3 and 0·4, except as noted in tables 4 and 5. Weights were obtained from the standard deviations of replicate runs at each shear rate. Larger uncertainties are obtained for smaller γ^* values. For $\gamma^{*1/2} < 0{\cdot}2$ the uncertainties in η^* are large enough to counterbalance their usefulness in extrapolating to $\gamma = 0$. Simulated values as a function of shear rate for many of the runs are shown in figures 5 and 6 along with the least squares fit of the data. At very high liquid densities, above about $\rho^* = 1{\cdot}8$, the region linear in $\gamma^{*1/2}$ was found to contract to

Table 4. Results of n-butane simulations.

		η^*					
T^*	ρ^*	$\gamma^* = 0{\cdot}16$	$\gamma^* = 0{\cdot}09$	$\gamma^* = 0{\cdot}0625$	$\gamma^* = 0{\cdot}04$	$\eta^*(0)$ (sim)	η^* (expt)
3·82	1·50	6·00	5·93	6·03	6·11	6·12	6·3
3·472	1·60	8·14	8·14	9·39	7·26	8·53	9·6
2·778	1·70	11·89	13·37	14·19	13·50	16·53	16·8
2·5	1·75	16·51	18·38	19·34	20·44	24·22	23·9
2·22	1·80	20·0	23·4	26·6	28·4	36·8	37·6
2·03	1·83	22·2	29·8	33·7	38·3	53·7	53·0
1·944	1·85	24·5[a]	34·7	40·9	47·0	71·6	73·0

[a]Value not used in linear extrapolation to $\gamma = 0$.

Table 5. Results of isobutane simulations.

		η^*					$\eta^*(0)$	η^*
T^*	ρ^*	$\gamma^* = 0.16$	$\gamma^* = 0.09$	$\gamma^* = 0.0625$	$\gamma^* = 0.04$	$\gamma^* = 0.0225$	(sim)	(expt)
4·167	1·55	5·76	5·76	5·89	5·35		5·7	5·50
3·472	1·68	9·22	9·45	9·58	9·35		9·8	9·57
2·778	1·80	14·37	16·44	17·92	18·63		23·3	19·0
2·5	1·85	18·3	20·1	22·9	23·7		29·4	27·8
1·944	1·90	22·38	28·44	31·32	35·7	40·9	47·1	46·0
1·875	1·93		31·7	38·7	45·9		74·2	75·2
1·667	1·95		36·6	45·5	55·3		92·7	100
1·736	1·97		39·9[a]	47·3	59·4	70·9	107	144
1·736	1·99	30·5[a]	42·6[a]	50·2[a]	66·6	90·3	161	182

[a]Value not used in extrapolation to $\gamma = 0$.

lower shear rates. For example, at the highest densities used for isobutane simulations, only shear rates for $\gamma^{*1/2} \leqslant 0.2$ could be safely assumed to be in the linear region. Values at even lower shear rates were required to supplement these extrapolations as shown in figure 6, in spite of the larger uncertainties at the lower shear rates. The simulations at $\rho^* = 1.99$ roughly represent the upper limit at which linear extrapolation to $\gamma^* = 0$ is useful owing to the narrowing of the linear region.

Values for $\eta^*(\gamma)$ obtained from the simulations are given in tables 4 and 5. The conditions shown were arbitrarily selected from the available experimental conditions so as to cover a wide range of densities at fairly regular intervals. The data present a much stronger function of density than temperature, although a separation of the isotherms is evident in figure 4 at the higher densities. Where mesurements had been made on more than one isotherm for the desired density, an experimental point at a

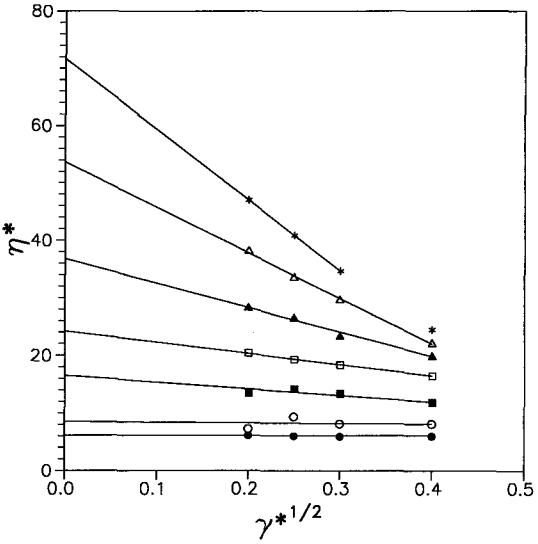

Figure 5. Results of n-butane simulations for $\eta^*(\gamma^{*1/2})$ at $\rho^* = 1.50$ (●), 1·60 (○), 1·70 (■), 1·75 (□), 1·80 (▲), 1·83 (△) and 1·85 (*). The T^* values for these points are listed in table 4. Lines represent weighted least squares fits through the data shown.

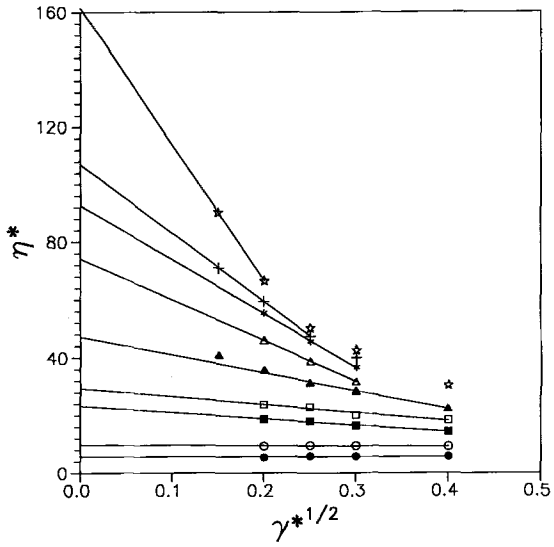

Figure 6. Results of isobutane simulations for $\eta^*(\gamma^{*1/2})$ at $\rho^* = 1{\cdot}55$ (●), 1·68 (○), 1·80 (■), 1·85 (□), 1·90 (▲), 1·93 (△), 1·95 (*), 1·97 (+) and 1·99 (☆). The T^* values for these points are listed in table 5. Lines represent weighted least squares fits through the data shown.

mid-range temperature was used as the comparison point. Also shown in these tables are the values of $\eta^*(0)$ obtained from the extrapolation procedure described above and from the experimental data [3]. A comparison of the density dependence of simulated and experimental η values is shown in figure 7. Simulated values agree remarkably well with the experimental data over the entire accessible density range.

The results are much less sensitive to ε, and the value used for n-butane was retained in the isobutane model. There is evidence, however, that a better value for

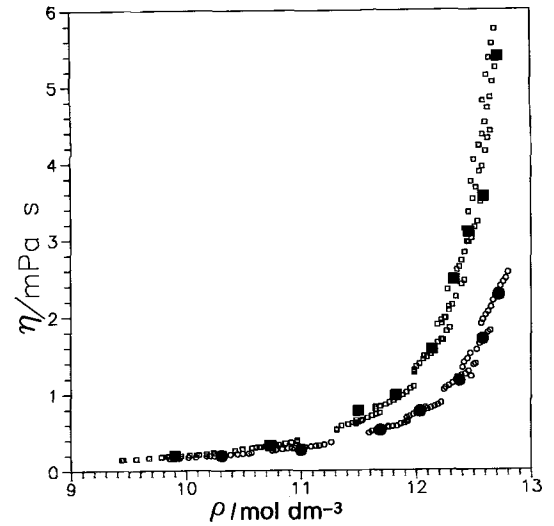

Figure 7. Comparison of simulated η values (filled symbols) with experimental data (empty symbols) [3] for n-butane (●, ○) and isobutane (■, □).

ε could be deduced from the data. Projections of the various experimental isotherms into the (η, ρ) plane shown in figure 7 are not quite coincident, particularly at higher densities. At the highest densities agreement between simulation and experiment actually appear to be better on this figure than that shown in table 5. This is because the simulated values are close to the experimental values for a different isotherm. It thus appears that T^* may be incorrectly scaled for isobutane. The simulated values appear to match higher isotherms at the same density, indicating that a larger value of ε is required to properly scale the temperature. This is consistent with the larger values of ε suggested by other models [7–10].

4. Discussion

The greater shear-thinning behaviour of n-butane observed in figures 3, 5 and 6 can be understood in terms of molecular structure. Consider first the case of n-butane. Figure 8 is a histogram of the percentage of the molecules in which the projection of the central bond vector $\boldsymbol{b}$ between sites 2 and 3 into the (x, y) plane forms an angle Θ with the x axis. Figure 9 is a similar histogram, but in this case shows the angle Φ between the x axis and the projection of the end-to-end vector $\boldsymbol{e}$ (from site 1 to site 4) onto the (x, z) plane. Note that increasing shear rates increase the alignment of the molecules, to minimize their extension across shear planes. However, because the molecules are nonlinear, the peaks in Θ are shifted slightly from 0° and 180°. Similarly, the drag on the molecule can be minimized by orientation of the chains in the (x, z) plane, which minimizes extension of the end methyl groups across streamlines. The shear driving force supplies the energy required to compensate the free energy for the entropic decrease associated with preferential orientation of the molecules.

Shear birefringence, this shear-induced molecular alignment, can also be monitored

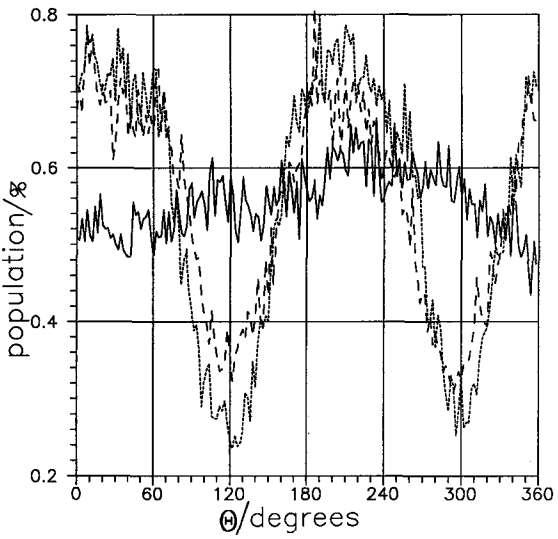

Figure 8. Histogram of percentage population of n-butane molecules whose central bond vector $\boldsymbol{b}$ projected into the (x, y) plane makes an angle Θ with the x axis. Results are shown for three values of the shear rate under the conditions of figure 3: ——, $\gamma^* = 0$; – – –, 0·04; - - - -, 0·25.

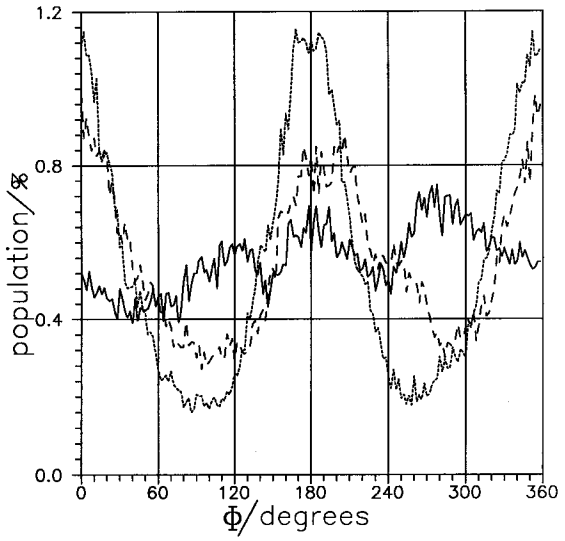

Figure 9. Histogram of percentage population of n-butane molecules whose end-to-end vector $\boldsymbol{e}$ projected into the (x, z) plane makes an angle Φ with the x axis. Results are shown for three values of the shear rate under the conditions of figure 3: ——, $\gamma^* = 0$; – – –, 0·04, – – – –, 0·25.

via the symmetric order tensor

$$\boldsymbol{S} = \frac{1}{N}\sum_i \boldsymbol{R}_i\boldsymbol{R}_i. \tag{15}$$

where the arbitrary orientation vector $\boldsymbol{R}_i$ is taken to be the end-to-end vector $\boldsymbol{e}_i$ for n-butane molecules and the bond vector $\boldsymbol{b}_i$ between a methyl group (site 1) and the central CH group (site 2) for isobutane molecules. It is convenient to examine this ordering effect in terms of the normalized birefringence or order tensor $\boldsymbol{S}^\circ = \boldsymbol{S}/\mathrm{Tr}(\boldsymbol{S})$. In an orientationally isotropic fluid $\boldsymbol{S}^\circ = \frac{1}{3}\boldsymbol{I}$. Figure 10 shows the diagonal and one off-diagonal components of $\boldsymbol{S}^\circ$, again indicating that the shear produces preferential orientation. From this figure it is apparent that the increasing alignment of the molecules in the shear field is a primary cause of the shear-thinning region noted in figure 3. The second rheological region in which the fluid viscosity is nearly independent of γ occurs when the orientational alignment is saturated. This is seen from figures 3 and 10 to occur at about $\gamma^* = 0{\cdot}25$. The values of S°_{zz} indicate that there is little tendency for butane molecules to align perpendicular to the shear plane and roll.

The alignment capability of isobutane due to a shear field is somewhat different than that of n-butane because of the inherent symmetry within the molecules. For isobutane the diagonal elements of $\boldsymbol{S}^\circ$ are all nearly $\frac{1}{3}$, independent of the shear rate. There is a slight orientation of the molecules, as indicated by the non-zero off-diagonal element S°_{xy} and the increase in S°_{zz} shown in figure 11. These small orientation alignments again saturate at about $\gamma^* = 0{\cdot}25$. Figure 12, analogous to figure 8, shows the orientation effects in terms of the percentage of molecules whose bond vectors (from the methyl group assigned as site 1 to the central CH group) form an angle Θ with the x axis when projected into the (x, y) plane. While these alignments

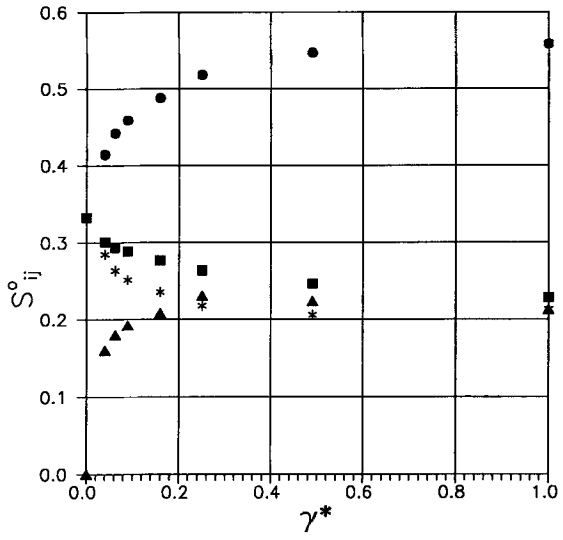

Figure 10. Components of the normalized order tensor for n-butane under the conditions of figure 3: ●, S°_{xx}; ■, S°_{yy}; ▲, S°_{xy}; *, S°_{zz}.

do produce shear-thinning rheology, the lack of large orientational alignment seen in n-butane accounts for the smaller slope observed in figure 3.

As observed in figure 4, the branched nature of isobutane produces a viscosity lower than that of n-butane at equivalent reduced conditions. Figure 3 indicates that the reduced viscosities are nearly equivalent at shear rates high enough to saturate molecular alignment capabilities within the fluid. It therefore seems likely that the higher reduced viscosity of n-butane at the lower shear rates is due to the extension

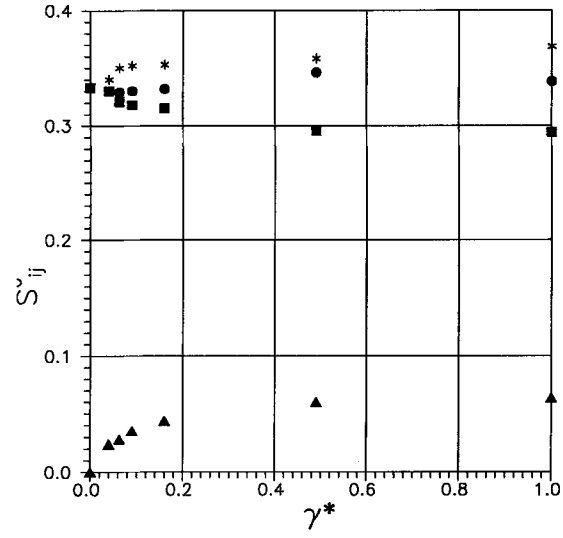

Figure 11. Components of the normalized order tensor for isobutane under the conditions of figure 3: ●, S°_{xx}; ■, S°_{yy}; ▲, S°_{xy}; *, S°_{zz}.

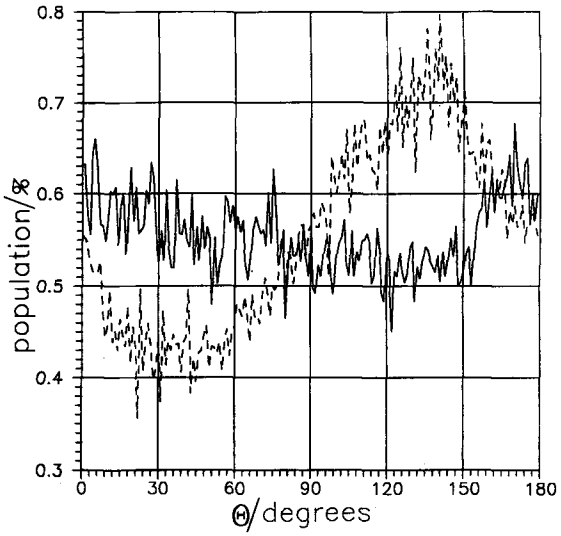

Figure 12. Histogram of percentage population of n-butane molecules whose bond vector $\boldsymbol{b}$ projected into the (x, y) plane makes an angle Θ with the x axis. Results are shown for two values of the shear rate under the conditions of figure 3: ——, $\gamma^* = 0$; – – –, 0·16.

of some of the chains over a wider range of shear rates in the y direction because of the random orientations. An alternative way of stating this is that the more branched molecule does not produce as much drag as the longer-chain molecules, some of which orient perpendicular to the shear. At higher shear rates, where orientational saturation occurs, the viscosities become approximately equivalent as the relatively lower alignment ability of the isobutane molecules takes its toll. A graphical simulation at $\gamma^* = 1{\cdot}0$ shows that oriented n-butane molecules are capable of a more independent movement in y layers, because the protruding methyl groups of the isobutane molecules tend to extend to different layers, locking the fluid into a more collective movement.

While current CS methods do not include orientational effects, the experimental viscosity data of figure 1 can be made to conform using effective molecular LJ parameters regressed specifically to superimpose the viscosities of the two fluids at equivalent reduced conditions [22]. This indicates that a relationship between the geometry of the molecule and effective molecular reducing parameters might be found that would improve the performance of the CS methods.

5. Conclusions

The structural difference between n-butane and isobutane does not produce the observed difference in viscosity at the same reduced conditions. Viscosities obtained from model I for isobutane are lower than those obtained from the n-butane model at equivalent conditions. However, the high-density region is particularly sensitive to the LJ size parameter σ used in the model, and viscosity data in this region can be used to regress accurate potential parameters. If the site size is increased by only 2·5% (model II), the CS scaling predominates and reverses the relative values of the reduced viscosity of the two fluids at equivalent conditions, in agreement with experiment. Simulations treating n-butane and isobutane as rigid molecules with four equivalent

sites are in excellent agreement with experimental data over the entire density range accessible to simulations with the methods used here when model II is used for isobutane. Interestingly, if figure 7 is plotted as $\eta^*(\rho^*)$, the n-butane and isobutane curves switch relative positions. The predominance of the scaling effect indicates that current CS theories might be improved. However, site rather than molecular scaling is used here. One would need to find a relationship between normal CS scaling parameters and the geometry of the molecule. Additionally, the purely structural effect upon the viscosity observed in these simulations would require additional study to completely correct CS theories. Some efforts in extending corresponding states theory to include orientation–translation coupling for rough hard spheres have produced good results in this area [23].

The inherent structural differences between the two molecules also produce differences in rheology. The shear-induced birefringence or alignment of the n-butane molecules accounts for its greater shear-thinning. This alignment capability is a function of shear rate, and in fact saturates at about $\gamma^* = 0{\cdot}25$. At higher shear rates (up to $\gamma^* = 1{\cdot}0$) the viscosity of both model fluids is nearly independent of shear rate. As extrapolation to $\gamma^* = 0$ is required to predict the experimental shear viscosity, it is crucial to identify the region over which (12) is valid when simulating structured molecules.

The code used in this work was modified from that used by Edberg *et al.* [5, 6]. We are grateful to Roger Edberg and Dennis Evans for use of their code. Gratitude is also expressed to NIST for the sabbatical opportunity of R.L.R. and his use of the supercomputer during that time. The very helpful suggestions and comments of Howard Hanley and Dan Friend, both of NIST, are also appreciated.

References

[1] Ely, J. F., and Hanley, H. J. M., 1981, *Ind. Engng Chem. Fundam.*, **20,** 323.
[2] Okeson, K. J., and Rowley, R. L., 1991, *Int. J. Thermophys.*, **12,** 119.
[3] Diller, D. E., and Van Poolen, L. J., 1985, *Int. J. Thermophys.*, **6,** 43.
[4] Ryckaert, J.-P., and Bellemans, A., 1978, *Discuss. Faraday Soc.*, **66,** 95.
[5] Edberg, R., Evans, D. J., and Morriss, G. P., 1986, *J. chem. Phys.*, **84,** 6933.
[6] Edberg, R., Morriss, G. P., and Evans, D. J., 1987, *J. chem. Phys.*, **86,** 4555.
[7] Maréchal, G., Ryckaert, J.-P., and Bellemans, A., 1987, *Molec. Phys.*, **61,** 33.
[8] Rebertus, D. W., and Berne, B. J., 1979, *J. chem. Phys.*, **70,** 3395.
[9] Ryckaert, J.-P., and Bellemans, A., 1975, *Chem. Phys. Lett.*, **30,** 123.
[10] Brown, D., and Clarke, J. H. R., 1983, *Chem. Phys. Lett.*, **98,** 579.
[11] Maréchal, G., and Ryckaert, J.-P., 1983, *Chem. Phys. Lett.*, **101,** 548.
[12] Jorgensen, W. L., Madura, J. D., and Swenson, C. J., 1984, *J. Am. chem. Soc.*, **106,** 6638.
[13] Evans, D. J., and Morriss, G. P., 1984, *Phys. Rev.* A, **30,** 1528.
[14] Evans, D. J., and Morriss, G. P., 1984, *Comput. Phys. Rep.*, **1,** 297.
[15] Ryckaert, J.-P., Ciccotti, G., and Berendsen, H. J. C., 1977, *J. comput. Phys.*, **23,** 327.
[16] Evans, D. J., Hoover, W. G., Failor, B. H., Moran, B., and Ladd, A. J. C., 1983, *Phys. Rev.* A, **28,** 1016.
[17] Street, W. B., Tildesley, D. J., and Saville, G., 1978, *Molec. Phys.*, **35,** 639.
[18] Kawasaki, K., and Gunton, J. D., 1973, *Phys. Rev.* A, **8,** 2048.
[19] Evans, D. J., 1983, *J. chem. Phys.*, **78,** 3297.
[20] Evans, D. J., Hanley, H. J. M., and Hess, S., 1984, *Phys. Today*, **37,** 26.
[21] Evans, D. J., 1981, *Phys. Rev.* A, **23,** 1988.
[22] Friend, D. G., 1990, Personal communication.
[23] Chandler, D., 1975, *J. chem. Phys.*, **62,** 1358.